

RESEARCH ARTICLE

# Angle amplifier in a 2D beam scanning system based on peristrophic multiplexed volume Bragg gratings

Yuanzhi Dong<sup>1,2,3</sup>, Yunxia Jin<sup>1,3,4</sup>, Fanyu Kong<sup>1,3</sup>, Jingyin Zhao<sup>1,3</sup>, Jianwei Mo<sup>1,3</sup>, Dongbing He<sup>1,3</sup>, Jing Sun<sup>1,3</sup>, and Jianda Shao<sup>1,2,3,4,5</sup>

<sup>1</sup>Thin Film Optics Laboratory, Shanghai Institute of Optics and Fine Mechanics, Chinese Academy of Sciences, Shanghai, China

<sup>2</sup>School of Physical Sciences, University of Science and Technology of China, Hefei, China

<sup>3</sup>Key Laboratory of High Power Laser Materials, Shanghai Institute of Optics and Fine Mechanics, Chinese Academy of Sciences, Shanghai, China

<sup>4</sup>CAS Center for Excellence in Ultra-intense Laser Science, Chinese Academy of Sciences, Shanghai, China

<sup>5</sup>Hangzhou Institute for Advanced Study, University of Chinese Academy of Sciences, Hangzhou, China

(Received 9 September 2022; revised 29 November 2022; accepted 14 December 2022)

## Abstract

In this paper, a 2D angle amplifier based on peristrophic multiplexed volume Bragg gratings is designed and prepared, in which a calculation method is firstly proposed to optimize the number of channels to a minimum. The induction of peristrophic multiplexing reduces the performance difference in one bulk of the grating, whereas there is no need to deliberately optimize the fabrication process. It is revealed that a discrete 2D angle deflection range of  $\pm 30^\circ$  is obtained and the relative diffraction efficiency of all the grating channels reaches more than 55% with a root-mean-square deviation of less than 3.4% in the same grating. The deviation of the Bragg incidence and exit angles from the expected values is less than  $0.07^\circ$ . It is believed that the proposed 2D angle amplifier has the potential to realize high-performance and large-angle beam steering in high-power laser beam scanning systems.

**Keywords:** beam scanning; high-power lasers; volume Bragg gratings

## 1. Introduction

Due to the outstanding performance in terms of the size, agility and reliability of non-mechanical beam steering devices, they play an important role in optoelectronic systems such as laser radar, free-space laser communication, laser weapons and laser countermeasures<sup>[1,2]</sup>. Various approaches have been explored to achieve non-mechanical beam steering control, including microlens arrays<sup>[3,4]</sup>, optical phased arrays based on dynamic liquid crystals (LCOPAs)<sup>[5–8]</sup>, integrated optical phased arrays<sup>[9–12]</sup>, liquid crystal prisms<sup>[13,14]</sup>, liquid crystal polarization gratings (LCPGs)<sup>[15–17]</sup>, liquid crystal polarization lenses (LCPLs)<sup>[18–20]</sup>, electro-optic deflectors<sup>[21,22]</sup>, etc. In high-power scenarios, it is still difficult for a single electro-

optic element to guarantee a high damage threshold while achieving wide-angle capability, which means that high-power beam steering systems face a great challenge with an insufficient deflecting angle. However, several different techniques for large-angle discrete steering (working as amplifiers) have been investigated. A technique based on birefringent prisms achieved a wide-angle capability of over  $20^\circ$ <sup>[23]</sup>. However, the thickness of the prisms increases significantly as the deflection angle becomes larger. Another wide-angle step-steering approach is based on LCPGs<sup>[16]</sup>. Multiple stages can be cascaded to implement a large-angle beam steerer. Nonetheless, with the increasing number of grating stages, the overall efficiency is obviously affected by steering efficiency, scattering, absorption and Fresnel loss. Recently, an angle amplifier realized by a telescope structure composed of LCPLs has also been developed rapidly<sup>[19,20]</sup>.

A volume Bragg grating (VBG) recorded in photo-thermo-refractive (PTR) glass has the advantages of high diffraction efficiency (DE) and excellent angle selectivity, as well as wavelength selectivity, flexible design and

Correspondence to: Fanyu Kong, Key Laboratory of Materials for High Power Laser, Shanghai Institute of Optics and Fine Mechanics, Chinese Academy of Sciences, Shanghai 201800, China. Email: kfanyu123@siom.ac.cn

high-power endurance, making it a good candidate as an angle amplifier in high-power laser beam scanning systems<sup>[24–28]</sup>. Raytheon Inc.<sup>[29]</sup> first proposed the structure of ‘LCOPA+VBG+LCOPA’ working as a 2D large-angle beam deflection system. The VBG amplifier is made of several multiplexed VBGs, and the grating vector plane of each VBG is perpendicular to the others. To the best of our knowledge, there are no reports of using peristrophic multiplexed volume Bragg gratings (PMVBGs) as 2D angle amplifiers as yet. Compared to the orthogonal approach, the proposed peristrophic multiplexing method realizes 2D angular deflection in the presence of only 1D angular deflection. It is possible for peristrophic multiplexing to reduce the performance difference caused by the parameter difference between channels in one bulk of the grating<sup>[30]</sup>, while there is no need to deliberately optimize the fabrication process, and it also simplifies the design and fabricating process. In this paper, three pieces of PMVBGs are designed based on a calculation method of optimizing the number of channels. Then the PMVBGs are fabricated by multiple exposures and subsequent heat treatment. It turned out that the PMVBGs are capable of discrete 2D angle deflection of  $\pm 30^\circ$ , and the maximum relative DE reaches more than 99%.

## 2. Theoretical design of volume Bragg gratings

### 2.1. Principle and calculation method

Peristrophic multiplexing, as a special angle multiplexing method, was firstly proposed to increase the capacity of holographic storage<sup>[31]</sup>. Its basic scheme is to keep the recording beam still and, every time a hologram is recorded, the recorded medium is rotated by an angle around its front surface normal axis. Applying peristrophic multiplexing in the design of the VBG amplifier, the recorded medium will have the capability of 2D angular deflection while maintaining the consistency of the parameters of each channel.

The scheme of the 2D beam scanning system based on PMVBGs is shown in Figure 1. Note that the LCOPAs should be capable of 2D beam deflection to ensure the incident beam couples into the corresponding grating channel. The control and amplification of the beam angle follow three steps. Firstly, the incident beam is deflected by a small angle (cone-shaped range) through the first stage addressing LCOPA. Then the beam is deflected to each amplified angle by the multiplexed VBGs. Finally, the second LCOPA finely controls and fills the beam at each exit angle (cone-shaped range). Here, to achieve continuous 2D coverage of the deflection angle, the angular intervals between two beams emitted from adjacent channels of the VBGs should all be within the deflection ability of the second LCOPA.

In the design process, the basic parameters of the VBGs include the incident angle as well as the corresponding exit angle of each channel, the rotation angle between each chan-

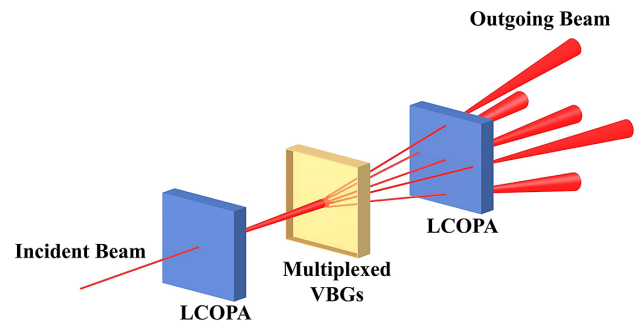


**Figure 1.** Scheme of the 2D beam scanning system. The incident beam (outgoing from the first stage addressing LCOPA) into multiplexed VBGs is first deflected to each amplified angle, then the second LCOPA finely controls and fills the beam in each exit angle. The LCOPA is capable of achieving precise angular deflection of the beam within the cone-shaped range.

nel and the number of channels. For a single grating channel, as shown in Figure 2(a), the incident beam is diffracted after passing through the VBG and amplified from  $\theta_i$  to  $\theta_o$  in the air. Four parameters mainly determine the diffraction characteristics of VBGs for a fixed wavelength: the Bragg incident angle ( $\theta'_i$ ), Bragg exit angle ( $\theta'_o$ ), grating period ( $\Lambda$ ), and grating slant angle ( $\varphi$ ). It is analyzed using the K-space diagram method according to Kogelnik’s coupled wave theory<sup>[32]</sup>. Here, the radius of the circle is  $\beta = 2\pi n_1/\lambda_1$ , where  $n_1$  is the normal index of refraction of the recorded material and  $\lambda_1$  is the working wavelength in free space. Two plane waves are presented and are referred to as the incident wave and diffracted wave, with wave vectors  $\rho$  and  $\sigma$ , respectively. The grating vector  $\mathbf{K} = \rho - \sigma$  is oriented perpendicular to the fringe planes and is of length  $|\mathbf{K}| = 2\pi/\Lambda$ . The Bragg condition is as follows:

$$\cos(\varphi - \theta'_i) = |\mathbf{K}|/2\beta. \quad (1)$$

When the Bragg condition is satisfied,  $\Lambda$  and  $\varphi$  are determined by the incident angle in the medium  $\theta'_i = \arcsin(\sin\theta_i/n_1)$  and the exit angle in the medium  $\theta'_o = \arcsin(\sin\theta_o/n_1)$ :

$$\begin{cases} \varphi = \frac{\pi}{2} + \frac{\theta'_i + \theta'_o}{2} \\ \Lambda = \frac{\lambda_1}{2n_1|\cos(\varphi - \theta'_i)|} \end{cases}. \quad (2)$$

The VBG is recorded at the recording wavelength  $\lambda_2$ , and  $n_2$  is the refractive index of the recording wavelength for the recording material. According to the interference principle, the following can be seen:

$$\begin{cases} \theta_B = \arcsin(\lambda_2/(2n_2\Lambda)) \\ \theta_s = \arcsin(n_2 \sin\theta'_s) = \arcsin(n_2 \sin(\varphi - \frac{\pi}{2} + \theta_B)) \\ \theta_r = \arcsin(n_2 \sin\theta'_r) = \arcsin(n_2 \sin(\varphi - \frac{\pi}{2} - \theta_B)) \end{cases}, \quad (3)$$

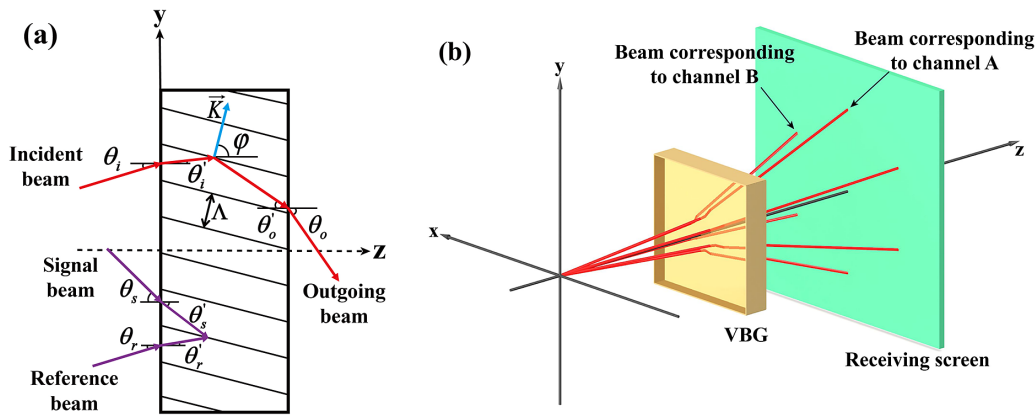


**Figure 2.** (a) Typical schematic of volume Bragg grating recording (purple line) as well as diffraction (red line), where the angle is positive when it is turned counterclockwise from the  $z$ -axis. (b) Schematic diagram of the beam emerging from the VBG, where the  $z$ -axis coincides with the front surface normal of the recording medium, channel-A corresponds to the channel with no rotation angle and channel-B corresponds to the channel with a rotation angle of  $\theta$ .

where  $\theta_B$  is the interference angle of the recording wavelength,  $\theta'_s$  and  $\theta'_r$  are the incident angles of the signal beam and the reference beam inside the medium, while  $\theta_s$  and  $\theta_r$  are the incident angles of the signal beam and the reference beam outside the medium, respectively.

As for the rotation angle between each channel and the number of channels, as shown in Figure 2(b), to describe the wave vector of the beam, it is assumed that the  $z$ -axis coincides with the front surface normal of the recording medium. The wave vector of the incident beam is expressed as follows:

$$\mathbf{k} = k_x \cdot \mathbf{x} + k_y \cdot \mathbf{y} + k_z \cdot \mathbf{z} = \begin{bmatrix} k_x \\ k_y \\ k_z \end{bmatrix}. \quad (4)$$

Assuming that the incident beam is along the  $z$ -axis, then its wave vector is as follows:

$$\mathbf{k} = \frac{2\pi n_1}{\lambda_1} \begin{bmatrix} 0 \\ 0 \\ 1 \end{bmatrix} = k_0 \begin{bmatrix} 0 \\ 0 \\ 1 \end{bmatrix}. \quad (5)$$

Now we set the rotation angle between adjacent channels of the grating to be  $\theta$ , that is, the rotation angle between channel-A and channel-B is  $\theta$ . After passing through a VBG, the wave vector of the beam will be as follows:

$$\mathbf{k}_1 = k_0 \begin{bmatrix} 0 \\ \sin \phi \\ \cos \phi \end{bmatrix}, \quad \mathbf{k}_2 = k_0 \begin{bmatrix} \sin \phi \sin \theta \\ \sin \phi \cos \theta \\ \cos \phi \end{bmatrix}, \quad (6)$$

where  $\phi$  is the angle between the beam and the  $z$ -axis,  $\mathbf{k}_1$  corresponds to channel-A and  $\mathbf{k}_2$  corresponds to channel-B. Similarly, after passing through an LCOPA, Equation (5) will

be rewritten as follows:

$$\mathbf{k}' = k_0 \begin{bmatrix} \sin \alpha \sin \gamma \\ \sin \alpha \cos \gamma \\ \cos \alpha \end{bmatrix}, \quad \alpha \in [0, \alpha_m], \quad \gamma \in [0, 2\pi]. \quad (7)$$

Here,  $\alpha_m$  is the maximum deflection angle of the LCOPA and  $\gamma$  is an arbitrary value representing the conical deflection range of the LCOPA. It is assumed that the LCOPA has the same deflection ability for different incident angles to simplify the calculation<sup>[33]</sup>. Then the wave vector of the beam emerging from the second LCOPA would be written as follows:

$$\begin{cases} \mathbf{k}'_1 = k_0 \begin{bmatrix} \sin \alpha \sin \gamma_1 \\ \sin \alpha \cos \gamma_1 \cos \phi + \cos \alpha \sin \phi \\ -\sin \alpha \cos \gamma_1 \sin \phi + \cos \alpha \cos \phi \end{bmatrix}, \quad \gamma_1 \in [0, 2\pi] \\ \mathbf{k}'_2 = k_0 \begin{bmatrix} \sin \alpha \sin \gamma_2 \cos \theta + \sin \alpha \cos \gamma_2 \cos \phi \sin \theta + \cos \alpha \sin \phi \sin \theta \\ -\sin \alpha \cos \gamma_2 \sin \theta + \sin \alpha \cos \gamma_2 \cos \phi \cos \theta + \cos \alpha \sin \phi \cos \theta \\ -\sin \alpha \cos \gamma_2 \sin \phi + \cos \alpha \cos \phi \end{bmatrix}, \quad \gamma_2 \in [0, 2\pi] \end{cases}, \quad (8)$$

where  $\mathbf{k}'_1$  corresponds to channel-A and  $\mathbf{k}'_2$  corresponds to channel-B, and the definitions of  $\gamma_1$  and  $\gamma_2$  are the same as  $\gamma$ . Here, some coordinate transformation skills are used. The value of  $\theta$  is determined by the proportion of coincidence of  $\mathbf{k}'_1$  and  $\mathbf{k}'_2$  (we see that they are two vector sets), which is defined as follows:

$$\mu = \frac{\mathbf{k}'_1 \cap \mathbf{k}'_2}{\mathbf{k}'_1 \cup \mathbf{k}'_2}. \quad (9)$$

It needs to be specified that  $\mu$  has to reach a certain value by adjusting  $\theta$  to ensure the continuity of the deflection, but blindly increasing  $\mu$  leads to a significant increase in the number of channels, which requires careful weighing.

### 2.2. Parametric design

The target deflection angle range for this beam scanning system is set as  $\pm 35^\circ$ , the working wavelength is 1064 nm

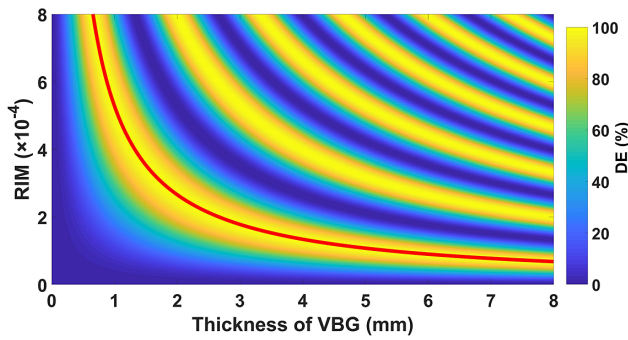


**Figure 3.** Relationship between grating thickness and diffraction efficiency as well as that between refractive index modulation and diffraction efficiency, under  $\theta'_i = 1.5^\circ$  and  $\theta'_o = 10^\circ$ . The red line corresponds to Equation (11).

and  $\mu$  and  $\alpha$  are set to 0 and  $5^\circ$ , respectively. In addition to the incident angle, the exit angle and rotation angle mentioned before, grating thickness ( $t$ ) and crosstalk should be focused on in the process of parametric design.

As high-level DE is expected, it is essential to balance the refractive index modulation (RIM) of each channel and the thickness of the grating. The DE  $\eta$  given by Kogelnik's coupled wave theory<sup>[32]</sup> is as follows:

$$\begin{cases} \eta = \frac{\sin^2(v^2 + \xi^2)^{1/2}}{1 + (\xi/v)^2} \\ v = \frac{\pi \Delta n t}{\lambda_1 (\cos \theta'_i \cos \theta'_o)^{1/2}} \\ \xi = \frac{\delta t}{2 \cos \theta'_o} \end{cases}, \quad (10)$$

where  $\delta$  is the phase mismatch factor and  $\Delta n$  is the RIM. Considering the upper limit of the dynamic range of PTR glass, one grating channel should achieve as high a DE as possible with lower RIM<sup>[34]</sup>. In the case of  $\delta = 0$  and  $v = \pi/2$ , the DE in Equation (10) will reach 100%, and accordingly we have the following:

$$\Delta n \cdot t = \frac{\lambda_1}{2} (\cos \theta'_i \cos \theta'_o)^{1/2} = \text{constant}, \quad (11)$$

which represents the rapidly decreased red line in Figure 3. It is considered that the RIM is not sensitive to the change of thickness when  $|d(\Delta n)/dt| < 10^{-4} \text{ (mm}^{-1}\text{)}$ . The thickness should be valued under the condition of satisfying this inequality so that one obtains a high DE with low RIM.

**Table 1.** Key parameters of the designed three VBGs.

Grating number	Rotation angle between channels $\theta$ ( $^\circ$ )	Peristrophic angular selectivity $d\theta$ ( $^\circ$ )	Number of channels	Incident angle in the air $\theta_i$ ( $^\circ$ )	Exit angle in the air $\theta_o$ ( $^\circ$ )	Grating period $\Lambda$ (nm)	Slant angle $\varphi$ ( $^\circ$ )	Thickness $d$ (mm)
VBG1	60	20.94	6	1.5	10	5318.1	92.84	3
VBG2	30	10.3	12	3	20	2685.1	95.62	3
VBG3	20	6.67	18	4.5	30	1820.2	98.28	4

Moreover, crosstalk may occur between channels due to the introduction of peristrophic multiplexing, so it is necessary to optimize the parameters of each channel. The angle selectivity of peristrophic multiplexing<sup>[31]</sup> is as follows:

$$d\theta = \left( \frac{2\lambda_1}{t} \left( \frac{\cos \theta'_o}{\sin \theta'_i (\sin \theta'_o + \sin \theta'_i)} \right) \right)^{1/2}. \quad (12)$$

When  $d\theta$  is larger than the rotation angle  $\theta$ , there will be a case of selective angle overlap, and then crosstalk occurs. To ensure that  $d\theta$  is small enough, the incident angle ( $\theta'_i$ ), exit angle ( $\theta'_o$ ) or grating thickness ( $t$ ) needs to be increased appropriately. In an angle amplifier,  $\theta'_o$  and  $\theta$  are fixed values, and  $t$  is related to the DE and RIM; hence, increasing the incident angle  $\theta'_i$  is a proper way to reduce  $d\theta$ , and crosstalk will be avoided as long as  $d\theta$  is much smaller than  $\theta$ .

Eventually, three VBGs for this system as an amplifier are designed, and the key parameters of each VBG are shown in Table 1. Note that the angular selectivity in the grating vector plane is less than  $0.12^\circ$  under the parameters given in Table 1 (a thick grating generally has narrow angle selectivity), which means that the crosstalk between VBGs is faint enough to be ignored because the angular interval between VBGs is much larger than the angular selectivity. As shown in Figure 4, when the incident angle and rotation angle of the incident beam are  $1.5^\circ$  and  $0^\circ$ , respectively, the beam will be deflected to point-M by VBG1. Similarly, the beam will be deflected to point-N by VBG2 when the incident angle and rotation angle of the incident beam are  $3^\circ$  and  $30^\circ$ , respectively. Thus, 2D angular amplification is achieved through three VBGs. With the purpose of realizing a  $35^\circ$  deflection range for the system, the LCOPA applied should provide a deflection range of at least  $5^\circ$ , and it also determines the angular resolution of the system, which is about several mrad<sup>[35,36]</sup>. It is possible for the overall transmission to reach more than 30% if the VBGs are lossless<sup>[18,23]</sup>.

### 3. Experimental details

To realize the proposed cascaded peristrophic multiplexed grating system, VBG1, VBG2 and VBG3 are fabricated and tested. After fabrication and testing of the three VBGs, they are integrated into one whole by refractive index matching liquid.

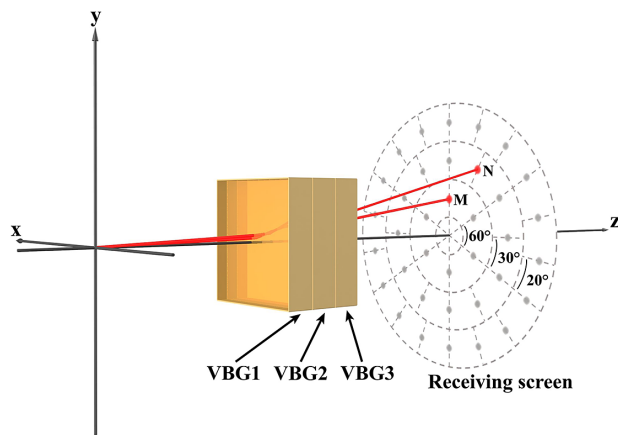


**Figure 4.** Schematic diagram of three VBGs working as an amplifier. The beam is deflected to point-M by VBG1 when the incident angle and rotation angle of the incident beam are 1.5° and 0°, respectively, and is deflected to point-N by VBG2 when the incident angle and rotation angle of the incident beam are 3° and 30°, respectively.

The fabrication process of each VBG based on PTR glass mainly contains two steps: sequential exposure and subsequent heat treatment. In the exposure process, the PTR glass is placed in an asymmetric dual-beam interference light field. In order to obtain the maximum contrast of interference fringes, an attenuator is inserted into one of the beams to ensure that the laser power of both beams is equal inside the medium. A He-Cd laser (Kimmon Electric Model IK3501R-G) with a wavelength of 325 nm and transverse electric (TE) polarization is used as the recording light source. The intensities of the two collimated beams are kept equal as required for obtaining maximum interference fringe contrast. Due to peristrophic multiplexing, the channels in the same gratings share the same light path setup. Take VBG1 for example, after the exposure of the first channel, the PTR glass is rotated by 60° around the normal of the grating surface, and then the second exposure is carried out as before to record a new channel. Therefore, three exposure setups with different interference angles are needed for the exposure of VBG1, VBG2 and VBG3. The exposure dosage of PTR glass samples for each channel is set to 60 mJ/cm<sup>2</sup> in VBG1, 30 mJ/cm<sup>2</sup> in VBG2 and 25 mJ/cm<sup>2</sup> in VBG3. After completing the exposure process, the samples are all heat-treated at 510°C for VBG1 for 1 h, VBG2 for 2.5 h and VBG3 for 2.5 h (the temperature is raised from 20°C with a heating rate of 10 K/min). The samples are finally polished to remove surface crystalline defects caused by heat treatment.

The scheme of DE measurement of multiplexed VBGs is shown in Figure 5. The sample is positioned on a motorized rotational stage with a step of 0.2686 mrad. A semiconductor laser source with a wavelength of 1064 nm, divergence of 0.48 mrad and waist diameter of 1.2 mm is used for testing. A linear polarizer is applied to select TE or transverse magnetic (TM) polarization and a beam expander is set

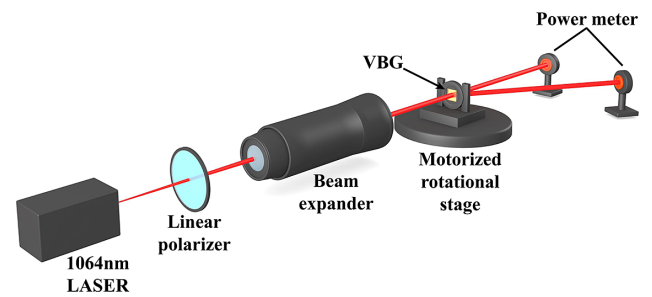


**Figure 5.** Scheme of DE measurement of multiplexed VBGs. The sample is positioned on a motorized rotational stage and different grating channels are tested using a sample stage, which allows the sample to be rotated around the front surface normal.

to reduce the divergence to 0.096 mrad. Different grating channels are tested using a self-made sample stage that allows the sample to be rotated around the front surface normal. The intensity of the transmitted zeroth-order beam ( $I_0$ ) is measured using a fixed power meter and that of the minus first-order diffracted beam of the different grating channel ( $I_{-1}$ ) is measured using an adjustable power meter (both Thorlabs, S120VC). The fixed power meter is placed in the direction of the transmitted zeroth-order beam and the adjustable one is placed in the direction of the diffracted beam. The testing process starts with rotating the sample around the front surface to the corresponding channel, and then angle scanning is implemented. A LabVIEW program is written to collect the angle and intensity data: each time the data is collected, the stage is rotated over a step. The relative DE is calculated as follows:

$$\eta_{\text{test}} = \frac{I_{-1}}{I_{-1} + I_0} \tag{13}$$

Due to peristrophic multiplexing, other channels may be read out when scanning one grating channel, but it does no harm to the calculation of DE; a detailed description can be found in the Supplementary Information.

In addition, the VBG recorded in PTR glass has a dual-channel characteristic, allowing us to measure the exit angle precisely and conveniently. The detailed mechanism is described in Ref. [30]. Still, it should be pointed out that the exit angle measured through this characteristic is always opposite to the designed value.

#### 4. Results and discussion

The respective performances of the fabricated multiplexed VBG1, VBG2 and VBG3 are tested individually. Figure 6(a) presents the DE and deviation from the expected Bragg angle of each channel in the three VBGs. Figures 6(b) and 6(c) give the angle selectivity curves (incident angle and exit angle, respectively) of the first channel in each monolithic grating and at the same time demonstrate the validity of

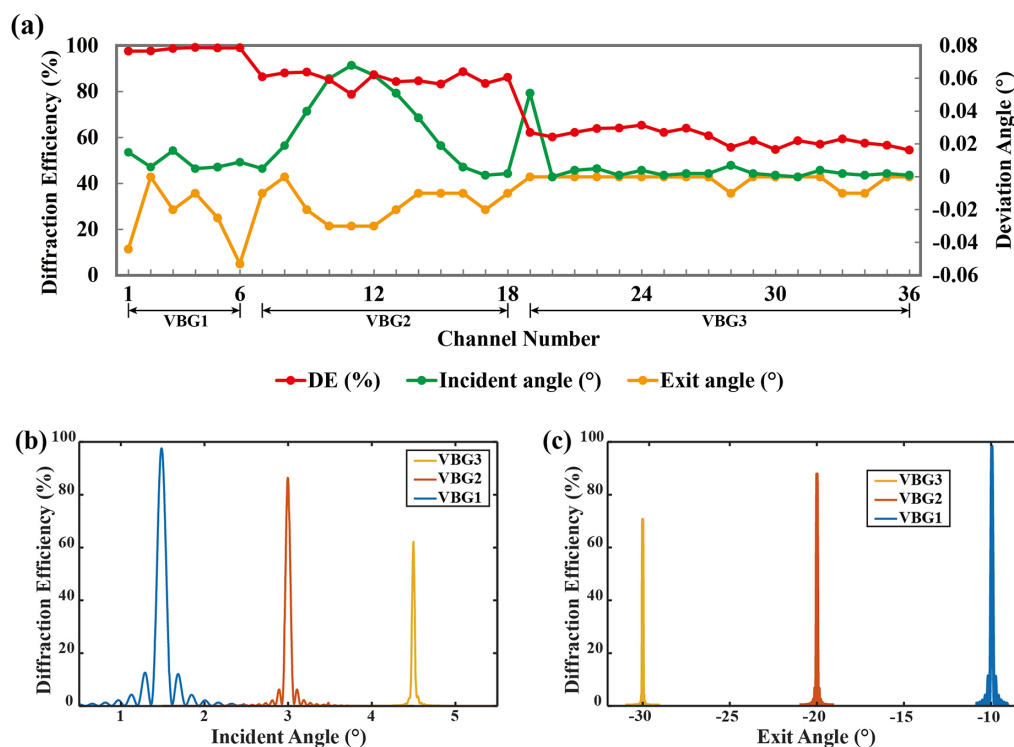


**Figure 6.** (a) DE and deviation angle of each channel. Experimental angle selectivity curves for the incident angle (b) and exit angle (c) of the first channel in each grating.

Equation (13), since the curves conform to the expected Bragg diffraction characteristics.

There is slight difference between the experimental and expected Bragg angles for all the grating channels, which is attributed majorly to the angle error in the interference exposure process and minorly to the sample positioning error both in the exposure process and the test process<sup>[30]</sup>.

For TE polarized incident light, the maximum DEs for the three VBGs are 99.18%, 88.64% and 65.36%, respectively. Subtle difference in DE between channels in the same grating (with a root-mean-square deviation of less than 3.4%) may result from the inhomogeneities of glass doping and the exposure field. The insufficient DE of VBG2 and VBG3 is thought to be due to the reduced exposure dosage, which leads to a low-level RIM<sup>[37,38]</sup>.

It is worth noting that there is no simple method to measure the exact RIM of the grating sample, so the most effective way is to fit the RIM of each channel through the DE curve of the sample. The fitting procedure of the RIM is consistent with Ref. [39], where a root-mean-square error function is applied to evaluate the coefficient of coincidence of the experimental and theoretical DE curves, which has a precision of approximately  $10^{-5}$  order of magnitude. Figure 7 shows the RIM fitting curve of the first channel of each monolithic VBG and its picture. Compared with VBG1, the extended heat treatment time of VBG2 makes up the reduced exposure dosage to a certain extent. The insufficient RIM of VBG3 mainly comes from the effect of gradient of refractive

index (GRIN)<sup>[40]</sup> since VBG2 and VBG3 have almost the same fabrication parameters but different thicknesses. The total RIM of a sample would be calculated by summing the RIM of each channel, which is  $1.16 \times 10^{-3}$  for VBG1,  $1.57 \times 10^{-3}$  for VBG2 and  $1.37 \times 10^{-3}$  for VBG3. Since the upper limit of the dynamic range of PTR glass is about  $2 \times 10^{-3}$ <sup>[34,41]</sup>, it is possible to have DE increased as long as the sample reaches a higher RIM.

The transmittances at 1064 nm of the three VBGs are tested to be 73.52%, 80.03% and 84.37%, respectively, through a spectrophotometer (PerkinElmer Lambda 950), and they could be enhanced by reducing the absorption of photo-reduced silver<sup>[42]</sup> and the scattering of  $\text{NaF}$ <sup>[43]</sup>.

Using several pieces of PTR glass to form a complete multi-channel is a simple way to improve the DE. For instance, VBG3 can be replaced by two pieces of 3 mm thick gratings with 9 channels. It is easier for nine-channel gratings to achieve a high DE since it is possible for each channel to allocate more modulation without worrying about the upper limit of the RIM. However, a more elegant way is assigning channels equally to three VBGs. As the number of channels in VBG1 is much fewer than that in VBG3, it is propitious to record part of the channels of VBG3 in VBG1.

Furthermore, in order to achieve a larger angular deflection range for the system, additional gratings with a larger exit angle need to be stacked, which may require more channels. It is foreseeable that dealing with more channels and maintaining a high DE will be the major challenges

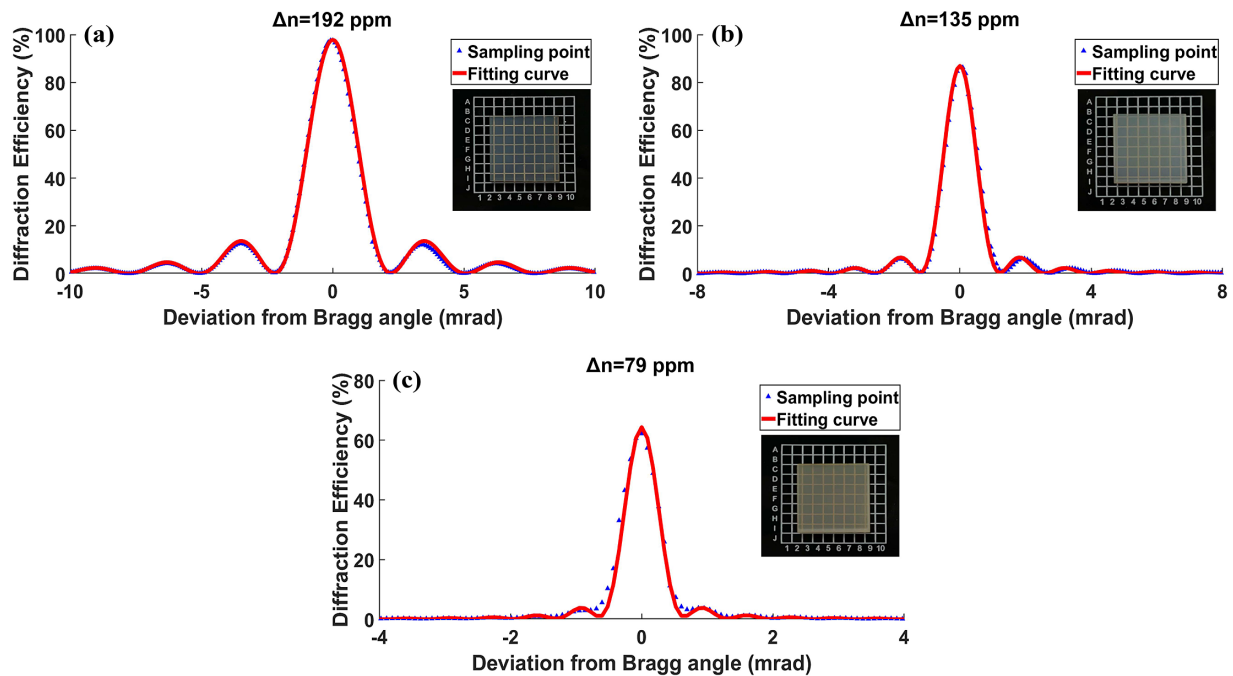


**Figure 7.** The RIM fitting curve of the first channel of each monolithic VBG and the corresponding picture. The total RIM of a sample would be calculated by summing the RIM of each channel, which is  $1.16 \times 10^{-3}$  for VBG1 (a),  $1.57 \times 10^{-3}$  for VBG2 (b) and  $1.37 \times 10^{-3}$  for VBG3 (c).

for the proposed 2D angle amplifier when facing a larger deflection range.

## 5. Conclusions

A 2D angle amplifier based on PMVBGs with a discrete 2D angle deflection range of  $\pm 30^\circ$  is designed and demonstrated. A calculation method is firstly proposed to optimize the number of channels to a minimum. The application of peristrophic multiplexing reduces the performance difference in one bulk of the grating, while no need to deliberately optimize the fabrication process. The results reveal that the maximum relative DE reaches more than 99%, while the minimum is about 55%, but there is only subtle difference in DE between channels in the same grating. The insufficient DE of VBG2 and VBG3 is thought to be due to the reduced exposure dosage. The deviation of the Bragg incident and exit angles from the expected values is less than  $0.07^\circ$ , and the total RIMs of the three VBGs are fitted to be  $1.16 \times 10^{-3}$ ,  $1.57 \times 10^{-3}$  and  $1.37 \times 10^{-3}$ , respectively. Assigning channels equally to multiple VBGs or dividing VBGs into multiple pieces of PTR glass is considered a proper way to improve the DE of the gratings. Further, the proposed method is flexible to adapt to a larger deflection range, which can be achieved by increasing the number of gratings and channels.

## Acknowledgements

This work was supported by the National Key R&D Program of China (No. 2020YFA0714500); the Shanghai Strategic Emerging Industry Development Special Fund

(No. 31011442501217020191D3101001); the National Natural Science Foundation of China (Nos. 61875212 and U1831211); and the International Partnership Program of Chinese Academy of Sciences (No. 181231KYSB20200040).

## Supplementary Materials

To view supplementary material for this article, please visit <http://doi.org/10.1017/hpl.2022.42>.

## References

1. R. Morris, C. Jones, and M. Nagaraj, *Micromachines* **12**, 247 (2021).
2. S. Lin, Y. Chen, and Z. J. Wong, *Nanophotonics* **11**, 2617 (2022).
3. A. Akatay and H. Urey, *Opt. Express* **15**, 4523 (2007).
4. R. Chen, Y. Shao, Y. Zhou, Y. Dang, H. Dong, S. Zhang, Y. Wang, J. Chen, B. F. Ju, and Y. Ma, *Nano Lett.* **22**, 1595 (2022).
5. P. F. McManamon, T. A. Dorschner, D. L. Corkum, L. J. Friedman, D. S. Hobbs, M. Holz, S. Liberman, H. Q. Nguyen, D. P. Resler, R. C. Sharp, and E. A. Watson, *Proc. IEEE* **84**, 268 (1996).
6. L. Wu, X. Wang, C. Xiong, Z. Huang, R. Zhuo, J. Rao, and Q. Tan, *Chin. Opt. Lett.* **15**, 101601 (2017).
7. S. Du, Y. Huang, C. Fu, and H. Guo, *J. Appl. Opt.* **38**, 581 (2017).
8. J. Hu, S. Du and H. Guo, *Laser Optoelectron. Prog.* **56**, 110002 (2019).
9. J. Sun, E. Timurdogan, A. Yaacobi, E. S. Hosseini, and M. R. Watts, *Nature* **493**, 195 (2013).
10. Y. Zhu, S. Zeng, and L. Zhu, *Photonics Res.* **8**, 375 (2020).

11. N. Alshamrani, A. Grieco, A. Friedman, K. A. Johnson, M. S. Kim, F. Floris, P. O'Brien, and Y. Fainman, *J. Light Technol.* **39**, 4201 (2021).
12. W. B. Lee, C. S. Im, C. Zhou, B. Bhandari, D. Y. Choi, and S. S. Lee, *Photonics Res.* **10**, 248 (2022).
13. F. Kimura, in *Proceedings of the International Display Workshops* (2012), p. 1227.
14. Z. W. Yu, B. Zhang, S. Y. Liu, Y. J. Wang, and J. G. Lu, *J. Disp. Technol.* **12**, 721 (2016).
15. J. Kim, C. Oh, S. Serati, and M. J. Escuti, *Appl. Opt.* **50**, 2636 (2011).
16. S. Serati, C. L. Hoy, K. Kluttz, J. Stockley, and C. Hale, *Opt. Eng.* **56**, 031211 (2016).
17. M. Sakamoto, H. T. Nhan, K. Noda, T. Sasaki, T. Kamei, T. Sakai, Y. Hattori, N. Kawatsuki, and H. Ono, *Appl. Opt.* **60**, 2062 (2021).
18. Z. He, F. Gou, R. Chen, K. Yin, T. Zhan, and S. T. Wu, *Crystals* **9**, 292 (2019).
19. Z. He, K. Yin, and S. T. Wu, *Light Sci. Appl.* **10**, 134 (2021).
20. Y. Li, Z. Luo, and S. T. Wu, *Crystals* **12**, 349 (2022).
21. R. W. Eason, A. J. Boyland, S. Mailis, and P. G. Smith, *Opt. Commun.* **197**, 201 (2001).
22. W. C. Wang and C. L. Tsui, *Sens. Actuators A Phys.* **188**, 277 (2012).
23. P. F. McManamon, P. J. Bos, M. J. Escuti, J. Heikenfeld, S. Serati, H. Xie, and E. A. Watson, *Proc. IEEE* **97**, 1078 (2009).
24. O. M. Efimov, L. B. Glebov, L. N. Glebova, K. C. Richardson, and V. I. Smirnov, *Appl. Opt.* **38**, 619 (1999).
25. Z. Yaqoob, M. A. Arain, and N. A. Riza, *Appl. Opt.* **42**, 5251 (2003).
26. A. L. Glebov, A. Sugama, V. I. Smirnov, S. Aoki, V. Rotar, M. G. Lee, and L. B. Glebov, *IEEE Photon. Technol. Lett.* **19**, 701 (2007).
27. L. Cao, Y. Zhao, Q. He, and G. Jin, *Proc. SPIE* **6832**, 683216 (2007).
28. F. Gao, X. Yuan, and X. Zhang, *Chin. Opt. Lett.* **14**, 060502 (2016).
29. I. W. Smith and M. K. O. Holz, U.S. Patent 7,215,472 (2007).
30. P. Chen, Y. Jin, D. He, J. Chen, J. Xu, J. Zhao, Y. Zhang, F. Kong, H. He, and J. Shao, *Opt. Express* **26**, 25336 (2018).
31. K. Curtis, A. Pu, and D. Psaltis, *Opt. Lett.* **19**, 993 (1994).
32. H. Kogelnik, *Landmark Papers on Photorefractive Nonlinear Optics* (World Scientific, Singapore, 1995).
33. L. Wu, X. Wang, C. Xiong, Z. Huang, Q. Tan, and M. Li, *Opt. Eng.* **55**, 116115 (2016).
34. S. Kaim, S. Mokhov, I. Divliansky, V. Smirnov, J. Lumeau, B. Y. Zeldovich, and L. B. Glebov, *J. Opt. Soc. Am. A* **32**, 22 (2015).
35. L. L. Tian, F. Chu, W. Duan, R. Li, X. Q. Gu, L. Li, and Q. H. Wang, *Opt. Commun.* **481**, 126525 (2021).
36. C. Wang, Q. Wang, Q. Mu, and Z. Peng, *Opt. Commun.* **506**, 127610 (2022).
37. J. Lumeau, L. Glebova, V. Golubkov, E. D. Zanotto, and L. B. Glebov, *Opt. Mater.* **32**, 139 (2009).
38. J. Lumeau and L. B. Glebov, *Opt. Mater. Express* **3**, 95 (2013).
39. P. Chen, D. He, Y. Jin, J. Chen, J. Zhao, J. Xu, Y. Zhang, F. Kong, and H. He, *Opt. Express* **26**, 157 (2018).
40. J. Lumeau and L. B. Glebov, *Appl. Opt.* **54**, 1587 (2015).
41. O. M. Efimov, L. B. Glebov, and H. P. Andre, *Appl. Opt.* **41**, 1864 (2002).
42. L. B. Glebov and V. I. Smirnov, *Proc. SPIE* **5273**, 396 (2004).
43. J. Lumeau, L. Glebova, and L. B. Glebov, *Opt. Mater.* **36**, 621 (2014).